ELSEVIER

Journal of Alloys and Compounds 293–295 (1999) 317–323

Journal of ALLOYS AND COMPOUNDS

A visible technology for display of hydrogen distribution in metals

Ming Au

Nanomaterials Research Corporation, Longmont, CO 80503, USA

Abstract

Tritium autoradiography provides the visible evidence of hydrogen distribution in the materials. The autoradiography of Ni base super alloys reveals that the hydrogen is trapped at grain boundaries, inclusions, interface of phases and particularly at high stress spots because of the strong local affinity to hydrogen. The conclusion that stress induces the hydrogen embrittlement which initiates from the crystal defects of materials has been proved by the visible evidence which was obtained from this work.

Keywords: Tritium autoradiography; Hydrogen distribution; Superalloy; Grain boundary

1. Introduction

Understanding the distribution of hydrogen in the microstructure of nickel based super alloys and stainless steels is important if efforts to minimize the effects of hydrogen embrittlement are to be implemented [1–3]. Tritium autoradiography can provide the direct and visible evidence of the hydrogen distribution complementing approaches used to calculate or estimate the behavior of hydrogen at the microscopic scale [4–7]. The vast majority of studies have been performed using ferrous alloys at ambient temperature. None have involved super alloys under the stress condition that plays an important role in stress corrosion cracking.

The purpose of this effort was to determine the microstructure features of materials that affect the local solubility of hydrogen. Six specimens of two materials (600, X750 super alloys) under three different conditions (nonstrained, strained and bolt-loaded notched) have been investigated. The necessary interpretations, especially on some unique and interesting phenomena, have been given.

2. Experimental details

2.1. Materials

Two Ni base super alloys (Inconel 600, X750) have been investigated in this work. Table 1 shows their chemical composition and heat treatment state.

2.2. Specimen preparation

The nonstrained specimens with 5×5×15-mm size were cut from the bulk materials. All strained specimens were cut from the 5% strained section of the tension specimens. Their dimension is φ 2.5×15 mm. One end of nonstrained and strained specimens were hand-ground to 600-grit strip of silicon carbide for tritium charge.

To ensure the stress without any change, the notched specimens with loading bolts were inserted to the charge cell wholly. After tritium charging, they were cut to 10×5×15 mm dimensions that cover the whole tip front area for grinding and polishing.

2.3. Tritium charge

Tritium charge was conducted in the radioactive protected glove box as shown in Fig. 1.

Tritium was introduced into the specimens by catholic charging in a tritiated molted salt solution. The initial amount of tritium was 10 Ci and a specific activity of 5 Ci/cm^3 was used. By-products of the tritiated solution were channeled through a series of condensers and bubbler traps to minimize the amount of released tritium and tritiated vapor. The molten salt consisted of 57% by weight $NaHSO_4$ (sodium bisulfate T_m=315°C) and 43% $KHSO_4$ (potassium bisulfate T_m=210°C). In this work, 1500 g mixed salt (2.03 g/ml bulk density) and 50 ml tritiated water (0.2 Ci/ml specific activity) were used. The eutectic mixture of salt starts to melt at 135°C. The tritium

0925-8388/99/$ – see front matter
PII: S0925-8388(99)00371-0

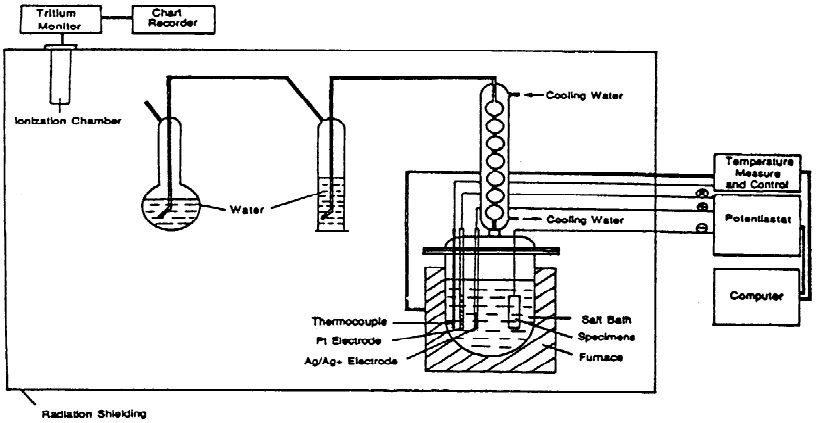

Fig. 1. Schematic diagram of tritium electrochemical charging facility.

Table 1
The composition and treatment of the super alloys to be observed

Materials	Composition (wt.%)							Heat treatment
	Ni	Cr	Fe	Ti	Al	Nb	C	
Inconel 600	78	16	6				<0.03	1065°C/1 h/air cool
Inconel X750	74	15	7	2.5	0.6	0.8	<0.03	1094°C/2 h/air cool 704°C/20 h/air cool

concentration of salt was 12.7 mCi/ml. Catholic charging took 3 h (4 h for compact tension specimens) under the 0.850 V Ag/Ag^{+} fixed potential and at 150°C with the specimens acting as the cathode. The electrochemical reactions that occurred in the tritium-charging cell are given as follows:

Anodic reaction: $H_3O^{+1} + 3SO_4^{-2} - 2e = 3HSO_4^{-1} + \frac{1}{2}O_2$

Catholic reaction: $HSO_4^{-1} + e = H + SO_4^{-2}$

The special multispecimens' holders were designed to introduce current and minimize the charge times. All specimens and holders except the charging surfaces were coated by thermal resistant silicone sealant to avoid galvanic reaction. After charging, the specimens were removed from the cell and rinsed with distilled water. The tritiated layer was then removed by hand-grinding with a 600-grit strip. The specimens remained in the radioactivity-proof glove box for 24 h to allow out-gassing of the diffusible tritium.

2.4. Surface polishing and etching

The charged specimens were polished step by step with 9 μ, 6 μ and 1 μ diamond paste under a fume hood. The super alloy specimens were etched by 3% Br–Methanol solution. The vacuum carbon coating was performed to reduce electron charge effect under scanning electron microscopy (SEM) and to protect the surface from chemical interaction with emulsion.

2.5. Film coating and processing

The L.4 type ILFORD emulsion with 140 nm average crystal diameter was selected as coating material. It was diluted by distilled water on the 1:1 volume ratio and heated at 40°C for 1 h with gentle steering (in a water bath). Then diluted emulsion was kept in the refrigerator (5°C) overnight for stabilization. Emulsion coating took place at 25°C and 60% humidity in a dust-free glove box. A film of emulsion was deposited on the specimen with the help of a thin wire expandable loop. Systematic controls were made by electron microscopy in order to ensure that the layer obtained is a close-packed monogranular arrangement of silver bromide grains.

After coating, the filtered nitrogen was introduced for 5 h to the dust-free glove box to dry the films. The coated specimens were set in a dry ice box (−78.50C) for 6 days for exposing the emulsion film by the β-ray emitted from remaining tritium in the materials (Fig. 2). After exposure, the irradiated silver bromide layer was processed directly

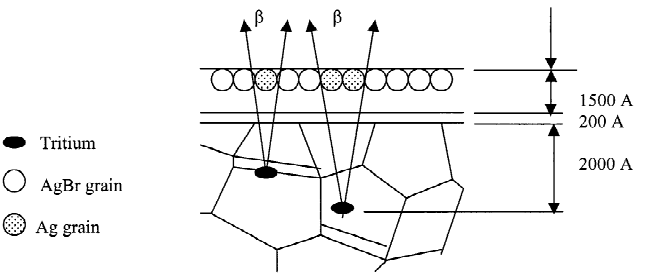

Fig. 2. Schematic picture of the depth of β-emission source and surface emulsion coating layer.

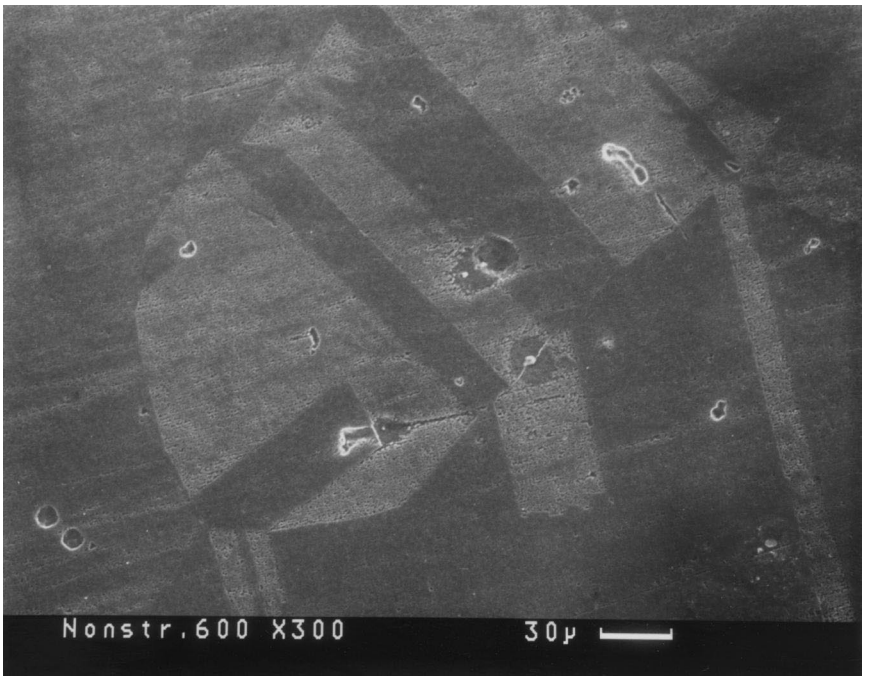

Fig. 3. Autoradiographic microstructure of nonstrained 600 super alloy. Hydrogen is trapped on the interface of inclusion and matrix (A); interface of carbides and matrix (B) and grain boundaries (C). ×300.

on the specimen by dipping for 4 min into the developer (Kodak D-19) and for 10 min into the fixer at 25°C. Then, the specimens were washed with distilled water for 10 min and dried in a dust-free box overnight.

2.6. SEM observation

The specimens were then directly observed in the SEM. The silver grains, resulting from the development of activated silver bromide grains, appeared in SEM images as white dots (about 1500 Å diameter) superimposed on the etched microstructure. The bromine released by active AgBr in the development of emulsion film broke the jelly and shaved the microstructure clearly (see Figs. 4 and 5).

As tritium is a low energy β-emitter ($E_{max} = 18$ keV), the radiation that reaches the AgBr layer is coming from a very thin layer under the surface (about 2000 Å). This fact added to the small diameter of the AgBr grains (1500 Å) leads to a very good resolving power for the method [8,9]. The average distance between the center of silver grain of the autoradiography and the tritium source that has generated it can be considered to be about 1200 Å, as Fig. 1 shows. For comparison, some optical microscope observations of uncoated specimens were also performed.

3. Results and discussion

3.1. Hydrogen traps in the nonstrained super alloys

For the annealed and unstrained Ni based super alloys, the autoradiography shows that hydrogen was trapped in certain microstructures. In the order of hydrogen intensity, these locations are: (1) the interface of inclusion and matrix as the arrow A indicated in Fig. 3; (2) the interface of primary carbides and matrix as the arrow B indicated in Fig. 3; (3) the grain boundaries on which carbides have precipitated as the arrow C indicated in Fig. 3. These observations evidence that the disordered interface area has more interstitial sites to attract and hold the hydrogen atoms.

3.2. Hydrogen traps in the strained super alloys

In these strained specimens, the intensity orders of hydrogen traps obviously differ from nonstrained ones because the tension stress forces the grains to slip and to rotate resulting in serious plastic deformation around the grain boundaries. The hydrogen traps in the order of their intensity are given as follows: (1) the deformed grain boundaries between the slipped grains as Figs. 4 and 5 show. This is a dominant kind of tritium trap in the strained 600 alloy; (2) the interface between carbides and matrix as arrow A marks in Figs. 5 and 6; (3) some special carbides that are rich in Ti or Nb elements as arrow B marks in Fig. 6. The EDX spectrum of carbide marked as B in Fig. 6 is given by Fig. 7. Some elements, such as Ti, Nb and Ta, possess a strong chemical affinity to build up hydrogen by means of chemical adsorption or reaction. The reactions, $Nb + 0.21H_2 = NbH_{0.42}$ and $Ta + 0.13H_2 = TaH_{0.26}$, will occur only under 0.1 MPa hydrogen pressure and at -48°C and 10°C respectively [10]. It is possible that the carbides that contain Ti, Nb and Ta become hydrogen traps by themselves [11–13].

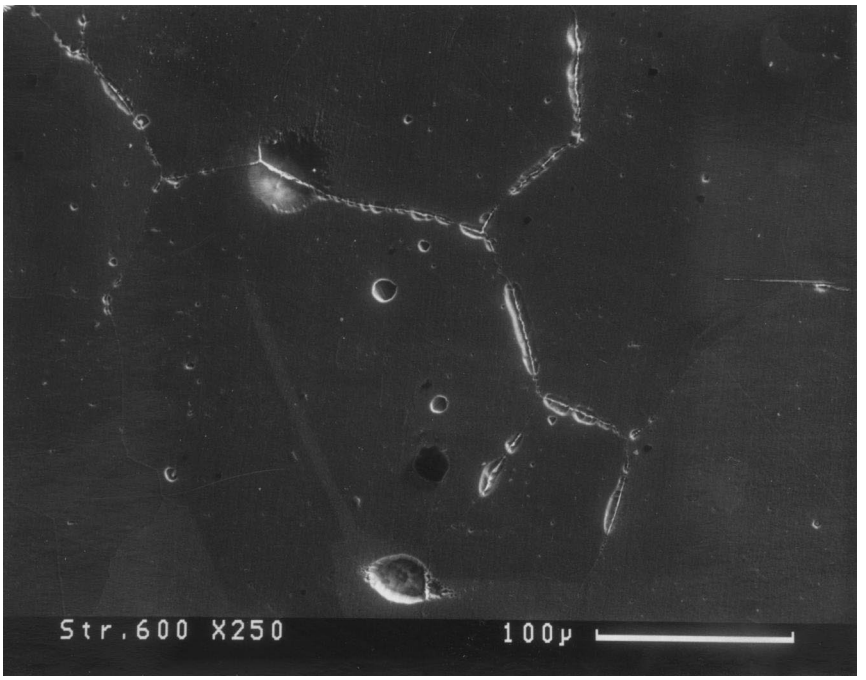

Fig. 4. Autoradiographic microstructure of strained 600 super alloy. Hydrogen is trapped on the deformed and slipped grain boundaries. ×250.

3.3. Hydrogen distribution under stress in the bolt-loaded notched specimens

The bolt-loaded notched specimens of 600 and X750 super alloys (Fig. 8) was charged with tritium under the stress. The tritium autoradiography of these specimens indicates that the stress and strain play an important role in the hydrogen distribution in material microstructure. Hydrogen concentrates in the seriously deformed and distorted grain boundaries. The load also causes high stress in the interface of different phases, such as interface carbides and matrix phase.

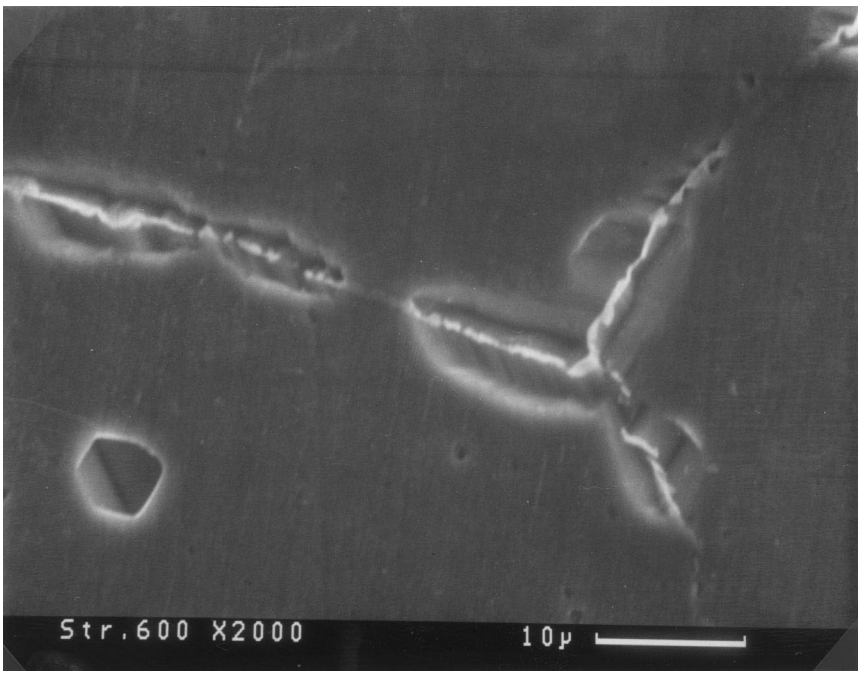

Fig. 5. Autoradiographic microstructure of strained 600 super alloy. Hydrogen is trapped on the deformed and slipped grain boundaries and interface between carbides and matrix. ×2000.

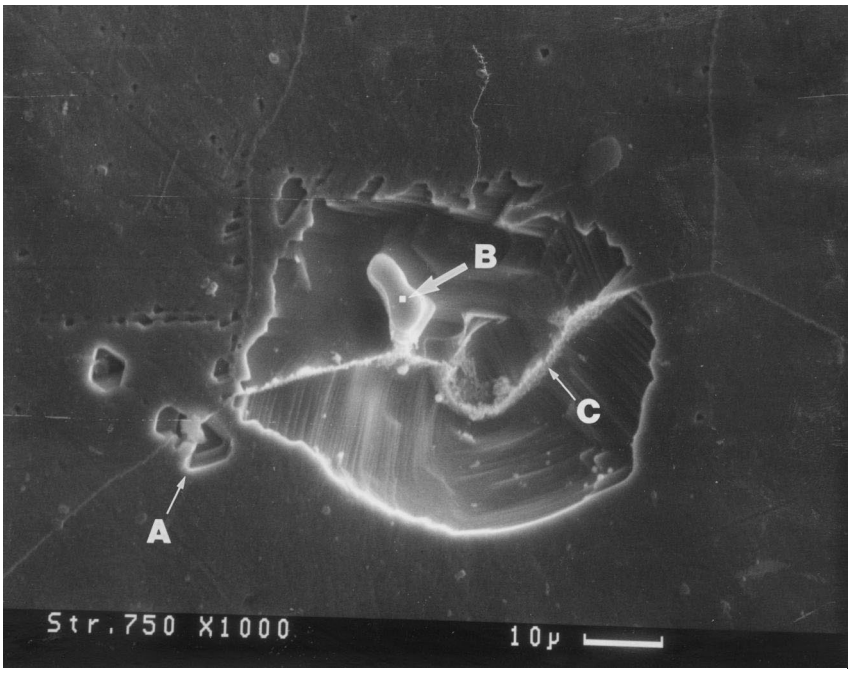

Fig. 6. Autoradiographic microstructure of strained 750 super alloy. Hydrogen is trapped on the interface of carbides and matrix (A); the carbides richen with Ti and Nb (B); deformed and distorted grain boundaries (C). ×1000.

The hydrogen traps in the order of their intensity are given as follows: (1) the grain boundaries deformed and distorted under the stress action, as shown in Fig. 9. These bright grain boundaries appear to peak ahead of notch corresponding to the maximum stress zone; (2) the primary carbides settled on the grain boundaries as shown in Fig. 10 (arrow A); (3) the interface of the primary carbides and matrix as shown in Figs. 9 and 10 (arrow B); (4) the intragranular primary carbides with micron voids as shown in Fig. 9 (arrow C).This void trapped hydrogen may initiate the decohesion of these particles with matrix under the assistance of stress [7]; (5) the twin boundaries as shown in Fig. 11 (arrow A).

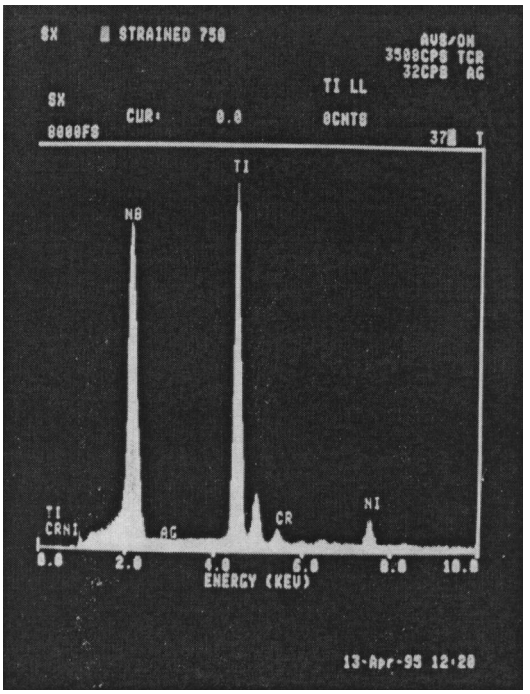

Fig. 7. EDX spectrum of the carbide B in Fig. 6.

4. Conclusion

Autoradiography has been successfully applied to the Ni based super alloys 600 and X750, under three stress conditions. This work is believed to be the first example where autoradiography has been used with notched specimens. The following summarizes the experimental findings:

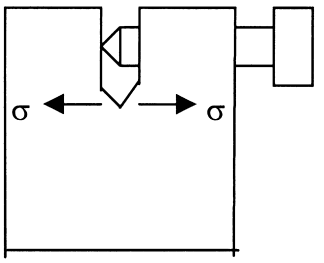

Fig. 8. The bolt-loaded notched specimen that has high stress in the front of notch tip.

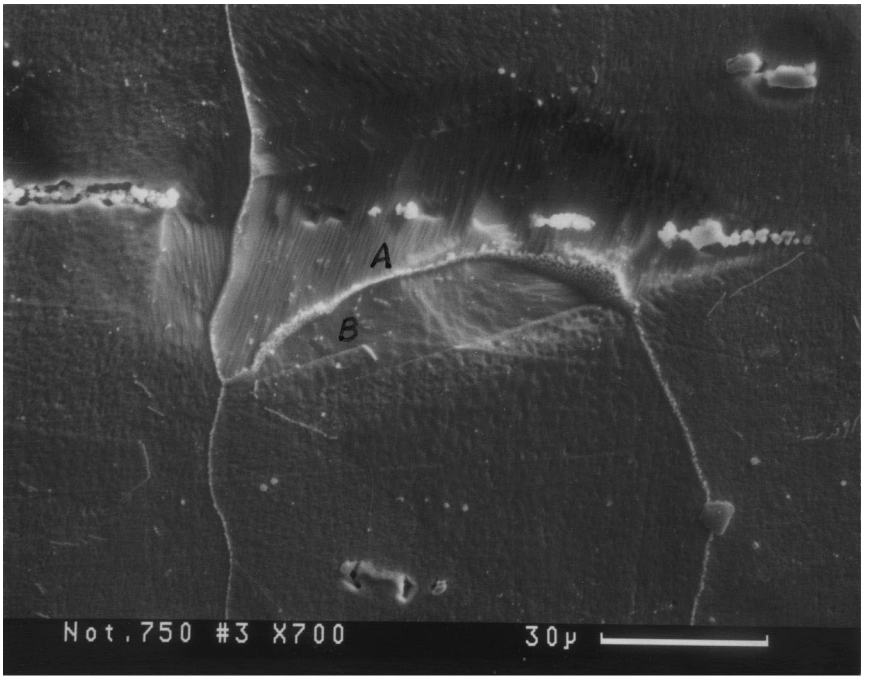

Fig. 9. Autoradiographic microstructure of the bolt-loaded notched specimen of 750 super alloy. Most hydrogen is trapped on the deformed and rotated grain boundaries (A) and twin boundaries formed by plastic deformation under stress action (B). ×700.

1. In the nonstrained specimens of X750 and 600 alloys, the interface of primary carbides and matrix is a dominant type of hydrogen trap. The carbides that are rich with Ti, Nb and Ta elements attract the tritium strongly by themselves. Some special grain boundaries in which tiny carbides deposit or primary carbides settle also trap some hydrogen.
2. In the strained specimens of X750 and 600 alloy, the deformed grain boundaries between the slipped grains are big tritium traps. The interface of the primary

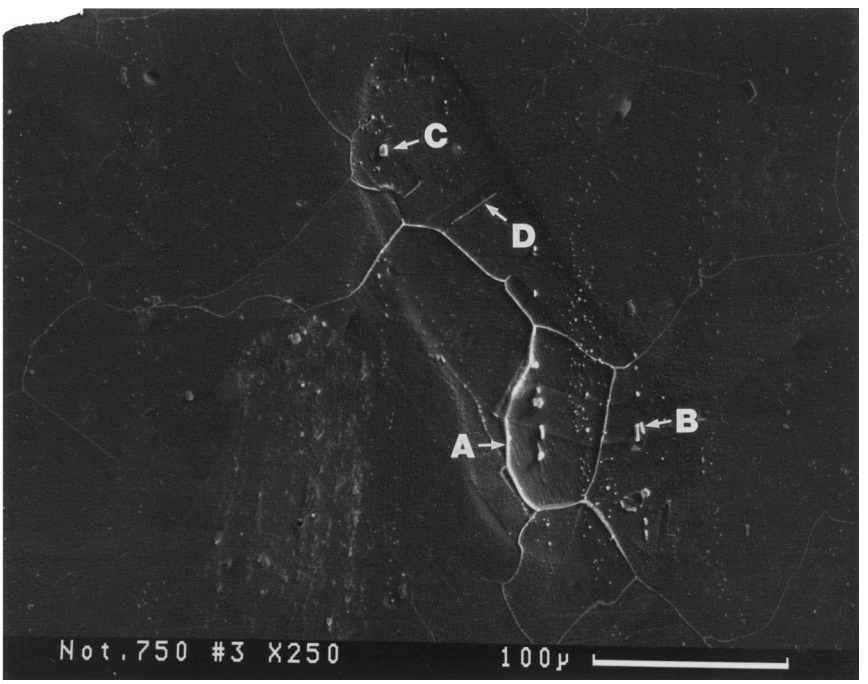

Fig. 10. Autoradiographic microstructure of the bolt-loaded notched specimen of 750 super alloy. Most hydrogen is trapped on the deformed and rotated grain boundaries (A); the twin boundaries formed by plastic deformation under stress action (B) and some hydrogen is trapped around the primary carbides also (C). ×250.

Fig. 11. The enlarged view of Fig. 10.

carbides and matrix and some special carbides rich in Ti, Nb and Ta elements are also found to trap the hydrogen in some degree.

3. In the notched specimens of X750 and 600 alloys, the deformed grain boundaries between the slipped (or rotated) grains are strong hydrogen traps. A notable fact is that some special points in grains become the hydrogen traps under stress action. They could be the dislocation tangles in which the stress is concentrated. It is a different behavior of hydrogen from those in the unloaded specimens. Similar to the unloaded specimens, the interface of the primary carbides and matrix and the carbides rich in Ti, Nb and Ta are also found to trap the hydrogen in some degree. There is enough visible evidence in this work to prove that the grain boundaries, interface of matrix and second phase, inclusion and stress centralized spots will trap the hydrogen and initiate the hydrogen embrittlement.

References

[1] Y. Shen, P.G. Shewmon, Corrosion (1991) (Sept) 712–718.
[2] D.M. Symons, Ph.D. thesis. Carnegie Mellon University, 1990.
[3] W.S. Walston, Ph.D. thesis. Carnegie Mellon University, 1990.
[4] B.A. Wilcox, G.C. Smith, Acta. Met. V12 (1964) 371–376.
[5] G.M. Pressouyre, Acta. Met. V28 (1980) 895–911.
[6] A.T. Festschrift, in: R. Gibala, R.F. Hehemann (Eds.), Hydrogen Embrittlement and Stress Corrosion Cracking, ASM, 1984.
[7] M.I. Baskes, C.F. Melius, Z. Phys. Chem. Neue Folge 116 (1979) 289–299.
[8] J.P. Laurent, G. Lapasset, Int. J. Appl. Isot. V24 (1978) 213.
[9] G.V. Prabhu Gaunkar, A.M. Huntz, P. Lacombe, Int. J. Appl. Rad. Isot. V30 (1979) 761.
[10] T. Massalski, Binary Alloy Phase Diagrams, ASM, 1993.
[11] R.L. Zanowick, W.E. Wallace, J. Chem. Phys. 36 (1962) 2059.
[12] W.E. Wallace, P. Kofstad et al., Pure Appl. Chem. 2 (1961) 281.
[13] G.G. Libowitz, The Solid-State Chemistry of Binary Metal Hydrides, W.A. Benjamin Inc., New York, 1965, pp. 23–49 and 91–113.